Solid State Science and Technology, Vol. 19, No2 (2011) 70-79
ISSN 0128-7389

SELF-ALIGNED PHOTONIC CRYSTAL VERTICAL-CAVITY SURFACE-EMITTING LASER BY PHOTOLITHOGRAPHY TECHNIQUE

Mohd Sharizal Alias[1]*, Sahbudin Shaari[2] and Dee Chang Fu[2]

[1]*Microelectronic & Nanotechnology Program, TMR&D, 63000 Cyberjaya, Selangor Malaysia*

[2]*Institute of Microengineering & Nanoelectronics, UKM, 43600 Bangi, Selangor*

**Corresponding author: sharizal@tmrnd.com.my*

ABSTRACT

In this paper, we report on single-mode operation of originally multi-mode oxide VCSEL by using etched photonic crystal air holes and unique trench structure. The device fabrication utilized conventional photolithography; with simplified lithography step of self-aligning the photonic crystal and trench structures to the laser aperture for efficient and vigorous device processing. The fabricated photonic crystal VCSEL with trench device exhibits a single-mode output power of 0.7 mW, threshold current of 3.5 mA, slope efficiency of 0.10 W/A, and continuous single-mode output spectra at wide operating current range. The results are compared with conventional multi-mode oxide VCSEL of similar device geometry. It is demonstrated that a highly confined and continuous single mode operation of VCSEL can be achieved by etching of photonic crystal air holes at the laser facet using a simple photolithography technique.

Keywords: Photonic crystal; VCSEL; Semiconductor laser;

INTRODUCTION

Vertical-Cavity Surface-Emitting Laser (VCSEL) are becoming primary light source for short data communication with the applications evolving into long wavelength optical telecommunication, optical interconnect, automotive network, optical mouse, gas spectroscopy, and high definition display [1-3]. The promising growth is due to VCSEL device superiorities of low operating current and power consumption, high fiber coupling efficiency, high modulation bandwidth, two-dimensional (2-D) arrays capability and most importantly the low-cost manufacturing ability (on wafer test and similar microelectronics device processing).

Single transverse mode operation of VCSEL is substantial for high coupling efficiency into a single-mode fiber which has small core diameter or for coupling into multi-mode fiber [4]. Standard multi-mode VCSEL at the moment used 10-20 μm oxide aperture technique for index- and current-confinement scheme [5, 6]. In order to attain single transverse mode operation, the oxide aperture of VCSEL must be smaller than 4 μm [7].

This rigorous requirement leads to low power output due to small oxide aperture, high optical losses due to scattering, and introduce high resistance which reduce the VCSEL high speed ability. Lately, various methods have been reported for achieving single transverse mode VCSEL by introducing losses to the higher-order modes such as proton implanted structure [8], surface-relief etching [9-11], hybrid oxide-implant VCSEL [12], holey structure [13-15], and photonic crystal air holes [16-25].

In this paper, we report on single-mode operation of originally multi-mode oxide VCSEL by using etched photonic crystal air holes and trench structure. The photonic crystal VCSEL (PhC VCSEL) with trench device fabrication utilized conventional photolithography with simplified self-align lithography step to ensure efficient and vigorous device processing. Also, we presented theoretical analysis (PhC model and mode profiles) based on the exact fabricated device properties. To the best of our knowledge, this is a first all-inclusive report on experimental work and theoretical analysis for this kind of PhC VCSEL (with trench and self-align photolithography process). Almost all of the previous reported PhC VCSEL is based on the air post mesa device structure [16-20] and used a complicated lithography process such as electron beam lithography [13, 17, 25, 26], focus ion beam lithography [19, 20], and chemically assisted ion beam lithography [18, 27].

EXPERIMENTAL DETAILS

Figure 1(a) shows the schematic device cross section of 850 nm PhC oxide VCSEL with trench structure. The VCSEL device consists of an active region of three GaAs quantum wells and four $Al_{0.3}Ga_{0.7}As$ barriers, embedded between 34.5 periods of bottom *n*-type and 25 periods of top *p*-type DBR mirrors. These DBRs composed of alternating high- and low-refractive index layers of $Al_{0.15}Ga_{0.85}As/Al_{0.9}Ga_{0.1}As$ multilayer. The oxidation layer is formed by a high aluminum concentration layer of $Al_{0.98}Ga_{0.02}As$. The n- and p-contact are materialized by metal alloys of AuGe/Ni/Au and Ti/Au, respectively.

Figure 1(b) illustrates the top view of the triangular lattice constant patterns with a single point defect at the center, used for the PhC design. Single-mode operation in PhC VCSEL can be realized similar to PhC optical fiber [28] by creating 2-D arrays of air holes onto the top DBR mirror. The PhC structure creates a step refractive index profile across the VCSEL device (perpendicular to the wafer plane). The PhC design parameters are connected by the triangular lattice constant, *a*, and air hole diameter, *b*. The transverse index guiding around the single defect point can be controlled by the air hole diameter to lattice constant ratio (*b/a*). We fixed the *b/a* ratio at 0.5 by defining a = 4 μm and b = 2 μm.

Solid State Science and Technology, Vol. 19, No2 (2011) 70-79
ISSN 0128-7389

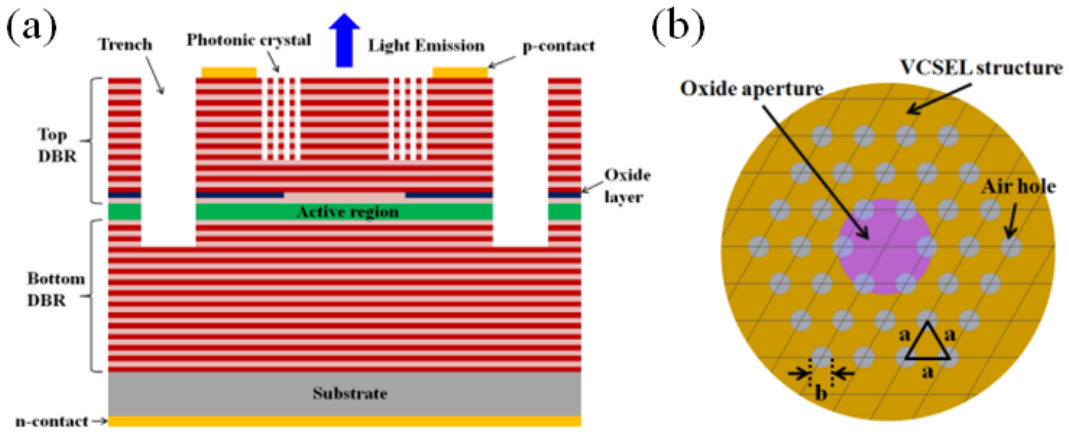

Figure 1: Schematic of (a) PhC VCSEL with trench cross section, and (b) PhC design top view

Figure 2 summarizes the main stages during the PhC VCSEL with trench device fabrication. The device fabrication started with metallization of the bottom n- and the top ring p-ohmic contacts by evaporating AuGe/Ni/Au (40/20/150 nm) and Ti/Au (15/150 nm), respectively. The top p-contact required photolithography patterning and lift-off process; however the bottom n-contact is a straightforward evaporation. The surface of the VCSEL epiwafer is proton implanted for device isolation. SiO_2 mask is deposited by the process of plasma-enhanced chemical vapor deposition (PECVD) followed by thick photoresist pillars coating on all VCSEL apertures for device protection prior to implantation. The photoresist is patterned by photolithography and SiO_2 mask is etched by reactive ion etching (RIE) for implantation. After implantation, the sample is cleaned by O_2 plasma and etched by RIE. Next, thick SiO_2 mask is re-deposited by PECVD. PhC holes and trench patterning (self-aligned) are then transferred by single-step photolithography to SiO_2 mask followed by RIE mask etched. The leftover photoresist is removed and thicker photoresist pillars are re-coated on top ring contacts to protect the PhC holes mask patterns prior to trench etching by inductively coupled plasma RIE (ICP-RIE). After trench is partly etched, the thick photoresist pillars are removed and sample is cleaned by O_2 plasma.

The epiwafer is then exposed to wet oxidation to form the oxide aperture. Next, PhC holes are etched onto the VCSEL aperture by second ICP-RIE process (trench will completely etched at the same time) followed by SiO_2 mask removal by RIE. The PhC VCSEL with trench device fabrication is completed by defining the fan-pad metal (formed by photolithography, Ti/Au of 25/1000 nm evaporation and metal lift-off). Typical oxide VCSEL with trench but without etched PhC holes is also fabricated (almost similar device processing but exclude PhC holes processing steps) to enable device comparison.

Solid State Science and Technology, Vol. 19, No2 (2011) 70-79
ISSN 0128-7389

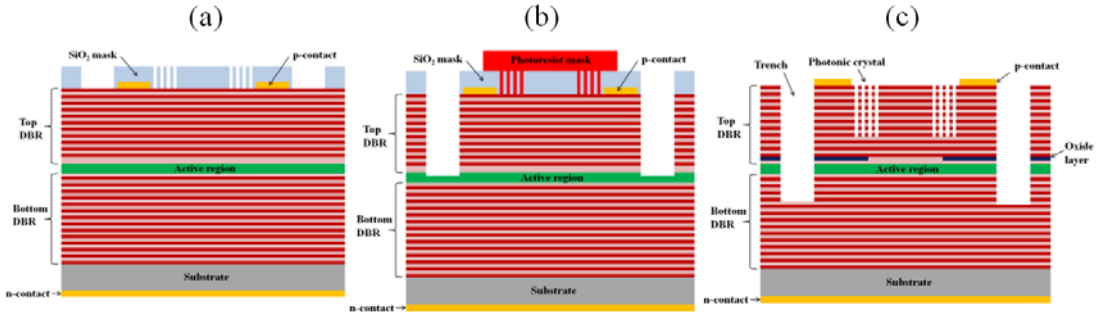

Figure 2: PhC VCSEL with trench device fabrication process of (a) PhC and trench patterns are transferred in single-step photolithography (self-aligned) to the SiO_2 mask, (b) first stage ICP-RIE for partial trench etching, and (c) second stage ICP-RIE for PhC holes etching and complete trench etching (after oxide layer is formed)

A self-aligned technique is utilized for aligning the PhC holes and trench structure by single-step photolithography. This approach allowed the PhC holes to be aligned automatically to the laser aperture with high accuracy for simplicity and reproducibility device processing. Figure 3 demonstrates the schematic top view of the PhC and trench single-step photomask (single step) and top ring contact photomask (separate step) along with a schematic cross section of a completed PhC VCSEL with trench device. By subtracting the inner diameter of the trench pattern (43 µm) with outer diameter of the top ring contact pattern (39 µm), it will give 4 µm alignment tolerance (2 µm at each half-side) which is sufficient for photolithography alignment.

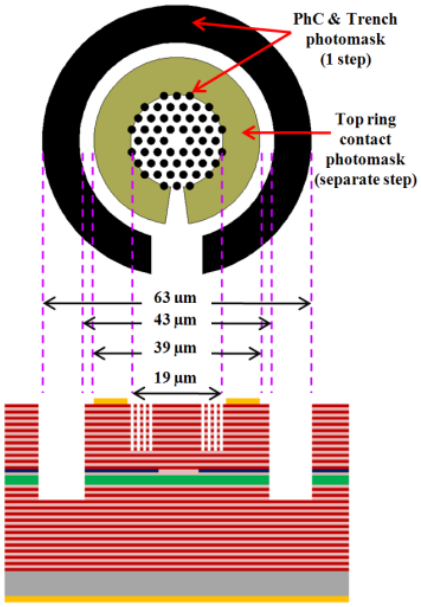

Figure 3: Schematic of self-align PhC & trench photomask along the fabricated PhC VCSEL with trench

Solid State Science and Technology, Vol. 19, No2 (2011) 70-79
ISSN 0128-7389

The device experimental measurement is performed on wafer probing system at room temperature under continuous wave operation. The light versus current (*L-I*) and current versus voltage (*I-V*) characteristics are measured with precise variation of input current (using semiconductor parameter analyzer). The light output is detected by a silicon photodetector which also is connected to the semiconductor parameter analyzer. The output spectrum of VCSEL is obtained by coupling the lasing beam into an optical fiber connected to an optical spectrum analyzer.

RESULTS AND DISCUSSION

Figure 4(a) shows the scanning electron microscope (SEM) image for the fabricated PhC VCSEL with trench of b/a = 0.5 (a = 4 µm and b = 2 µm). The PhC holes are perfectly etched onto the VCSEL top DBR with the unetched defect point at the center. The circular trench structure surrounding the VCSEL mesa is also well etched. It can be noticed that the PhC and trench pattern (single-step photomask) is slightly misaligned to the right of the top ring contact (initial step photomask). However, the PhC holes area is still within the VCSEL aperture (inner area of the top ring contact) due to sufficient alignment tolerance. This result shows the significance of the self-align technique used in order to ensure simplified, reproducible and vigorous PhC VCSEL with trench fabrication. Figure 4(b) and 4(c) shows the microscope image of PhC with trench single-step pattern, and fabricated PhC VCSEL device with trench, respectively.

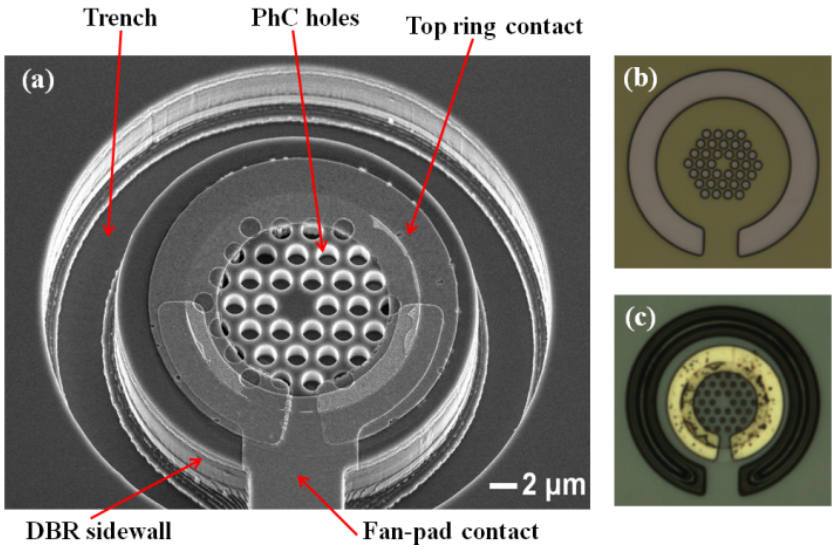

Figure 4: Top view microscopy images of (a) tilted SEM, (b) PhC with trench single-step patterning, and (c) fabricated device (prior to fan-pad metallization)

Figure 5(a) shows the *L-I-V* characteristic for PhC VCSEL with trench of b/a = 0.5 (a = 4 µm and b = 2 µm) and oxide aperture diameter of 9 µm. The fabricated device achieved threshold current, I_{th} of 3.5 mA, slope efficiency of 0.10 W/A, and output power, P_{max} of 0.7 mW. The *L-I-V* characteristic for the control device of oxide trench

VCSEL (without PhC holes) with similar oxide aperture diameter of 9 µm is shown in Fig. 5(b) for comparison. The device exhibited I_{th} of 0.8 mA, slope efficiency of 0.29 W/A, and P_{max} of 3.0 mW. The high I_{th} and low slope efficiency in PhC VCSEL with trench is because higher optical threshold gain is required to compensate high-order mode loss [18]. In addition, the etched PhC holes increased scattering loss [26] which also results in higher threshold current is required to ensure lasing. Also, PhC holes might lead to non-radiative recombination of the injected current [31]. Output power for PhC VCSEL with trench is low compared to control device since only fundamental mode is allowed for lasing and the laser emitting area is reduced due to the existence of PhC holes structure. However, the power composed of genuine single-mode operation. The output power can be improved by optimizing device parameters such as oxide aperture, etch depth and PhC design. From the slope of *I-V* characteristic, the differential series resistance, R_s of PhC VCSEL with trench is approximately 124 Ω. The control device R_s is approximately 87 Ω. The high series resistance of PhC VCSEL with trench is due to the current flow resistance induced by PhC holes and the etched trench structure. The etching of PhC holes partially removed the conductive p-doped material of the top DBR mirror.

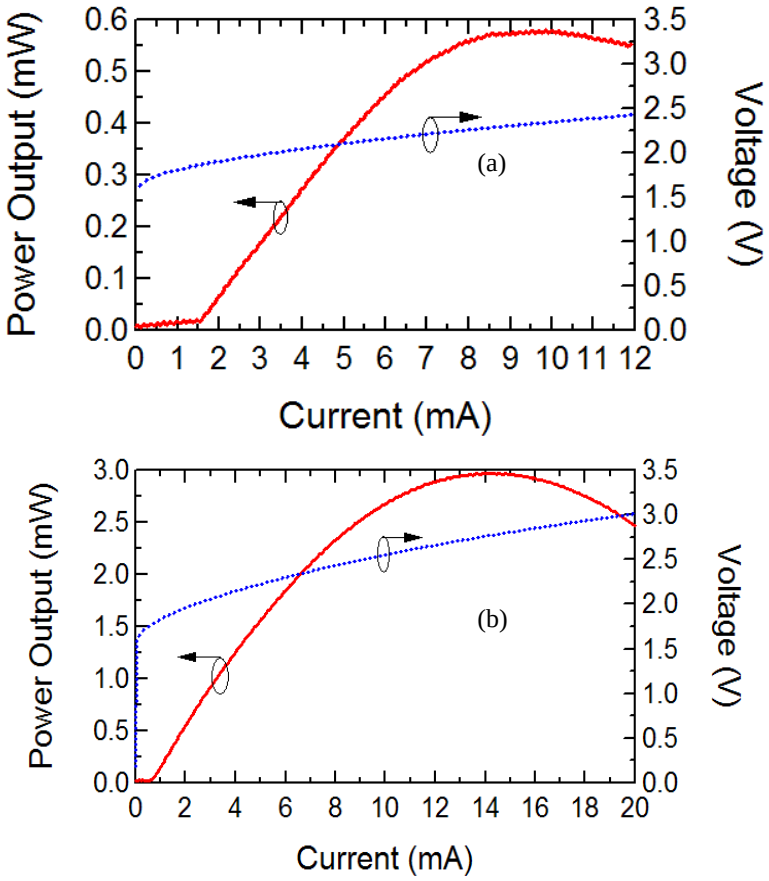

Figure 5: *L-I-V* characteristic of (a) PhC VCSEL with trench, and (b) typical VCSEL with trench

Figure 6 exhibits output spectrum for both PhC VCSEL with trench and control device above threshold. By combining PhC holes with trench structure in VCSEL, highly confined single-mode condition is obtained. Single-mode condition is defined if more than 30 dB difference in side mode suppression ratio (SMSR) is achieved from threshold to rollover lasing operation. The PhC VCSEL with trench demonstrates approximately 35 dB of SMSR. Also, it is observed that the lasing wavelength blue-shifted when PhC holes and trench are incorporated into the VCSEL. This effect could be donated by the change of VCSEL cavity resonance due to modification of top DBR refractive index when trench and PhC holes are etched into the semiconductors.

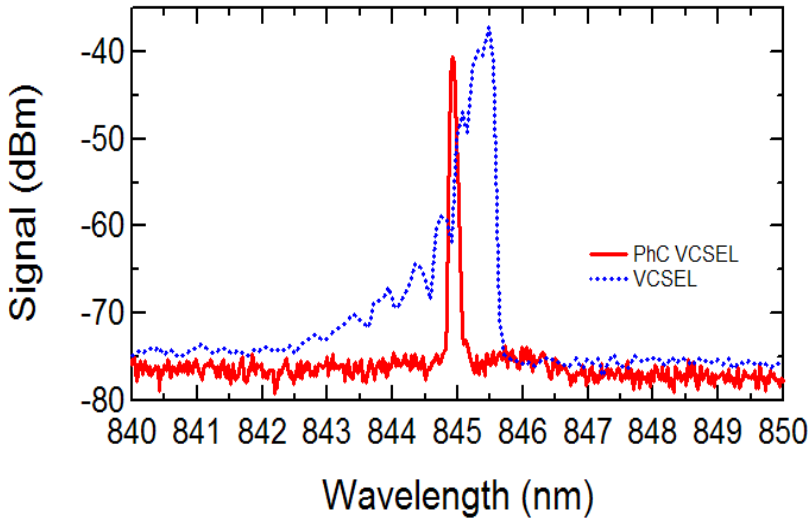

Figure 6: Output spectrum of PhC VCSEL with trench and typical VCSEL with trench

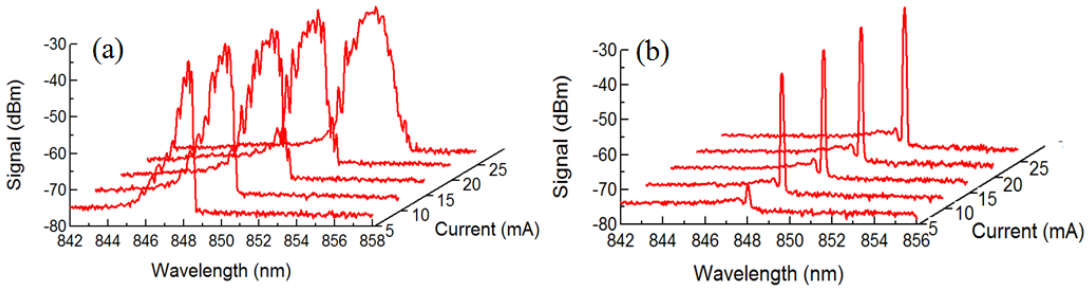

Figure 7: Output spectrum for (a) typical VCSEL, and (b) PhC VCSEL; at various injected current

Figure 7 exhibits the output spectrum for both VCSEL devices at increasing injected currents. PhC VCSEL with trench achieved single-mode condition (SMSR > 30 dB) and narrow linewidth throughout the operating current range (above threshold current). No distinguish side modes appear at even high operating current. The typical oxide VCSEL shows multimode spectrum from low to high injection current levels. Several

transverse modes existed within the operating wavelength range. The spectrum also exhibits broadening linewidth as the injected current increased. The peak lasing wavelength is red-shifted for both devices as injected current increased due to VCSEL self-heating effect (due to high number of heterojunctions).

The near-field optical image comparison for both VCSEL devices is shown in Figure 8. The PhC VCSEL with trench structure demonstrates superior laser beam confinement at the centre of the PhC structure (no defect point) throughout the operating current range. Higher-order modes are discriminated and only fundamental mode is allowed for lasing. As for the trench VCSEL without PhC holes, the laser beam is distributed across the entire VCSEL aperture. Due to this, the trench VCSEL exhibits a higher output power compared to PhC VCSEL.

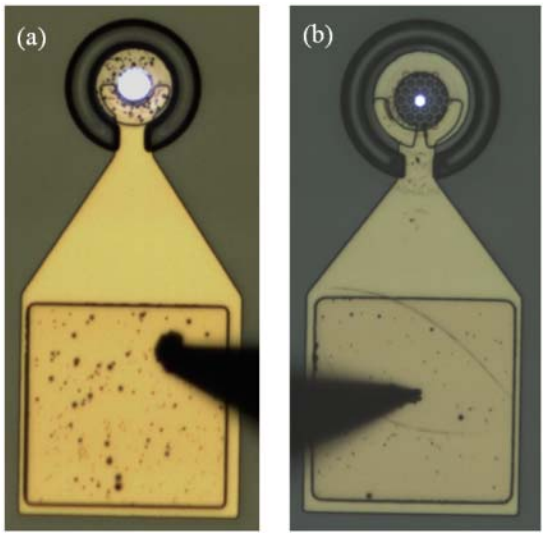

Figure 8: Near-field comparison for (a) trench VCSEL and (b) PhC VCSEL with trench

CONCLUSION

In this paper, we presented the output characteristics of PhC VCSEL with unique trench structure. The device is fabricated by conventional photolithography with simplified lithography step of self-aligning the photonic crystal and trench structure to the laser aperture. By this, we proposed an efficient, simplified and reproducible device processing for the intended device. The fabricated PhC VCSEL with trench device exhibits single-mode output power of 0.7 mW, threshold current of 3.5 mA, slope efficiency of 0.10 W/A, and continuous single-mode output spectra at wide operating current range. These device characteristics are compared with a control device (oxide multi-mode VCSEL with trench) for further analysis. Although the PhC VCSEL with trench exhibits lessen electrical characteristic (due to optical loss by PhC holes), the device achieved continuous single-mode operation throughout wide operating current and emitting genuine single-mode power.

REFERENCES

[1] K. Iga, *IEEE J. Quantum Electron.* **6** (6) (2000) 1201
[2] F. Koyama, *IEEE J. Lightwave Technol.* **24** (12) (2006) 4502
[3] C. W. Wilmsen, H. Temkin, and L. A. Coldren, *Vertical-Cavity Surface Emitting Lasers: Design, Fabrication, Characterization, and Applications* (Cambridge Univ. Press, Cambridge, UK, 1999).
[4] P. Pepeljugoski, D. Kuchta, Y. Kwark, P. Pleunis, and G. Kuyt, *IEEE Photon. Technol. Lett.* **14** (5) (2002) 717
[5] K. D. Choquette, K. L. Lear, R. P. Schneider, K. M. Geib, J. J. Figiel, and R. Hull, *IEEE Photon. Technol. Lett.* **7** (11) (1995) 1237
[6] B. Weigl, M. Grabherr, C. Jung, R. Jager, G. Reiner, R. Michalzik, D. Sowada, and K. J. Ebeling, *IEEE J. Sel. Topics Quantum Electron.* **3** (2) (1997) 409
[7] C. Jung, R. Jager, M. Grabherr, P. Schnitzer, R. Michalzik, B. Weigl, S. Muller, and K. J. Ebeling, *Electron. Lett.* **33** (21) (1997) 1790
[8] R. A. Morgan, G. D. Guth, M. W. Focht, M. T. Asom, K. Kojima, L. E. Rogers, and S. E. Callis, *IEEE Photon. Technol. Lett.* **4** (4) (1993) 374
[9] H. Martinsson, J. A. Vukusic, M. Grabherr, R. Michalzik, R. Jager, K. J. Ebeling, and A. Larsson, *IEEE Photon. Technol. Lett.* **11**(12) (1999) 1536
[10] A. Haglund, J. S. Gustavsson, J. Vukusic, P. Modh, and A. Larsson, *IEEE Photon. Technol. Lett.* **16** (2) (2004) 368
[11] E. Soderberg, P. Modh, J. S. Gustavsson, A. Larsson, Z. Z. Zhang, J. Berggren, and M. Hammar, *IEEE Photon. Technol. Lett.* **19** (5) (2007) 327
[12] E. W. Young, K. D. Choquette, S. L. Chuang, K. M. Geib, A. J. Fischer, and A. A. Allerman, IEEE Photon. *Technol. Lett.* **13** (9) (2001) 927
[13] A. Furukawa, S. Sasaki, M. Hoshi, A. Matsuzono, K. Moritoh, and T. Baba, *Appl. Phys. Lett.* **85** (22) (2004) 5161
[14] P. O. Leisher, A. J. Danner, J. J. Raftery, Jr., D. F. Siriani, and K. D. Choquette, *IEEE J. of Quantum Electron.* **42** (10) (2006) 1091
[15] H. P. D. Yang, I-C. Hsu, F.-I. Lai, H. C. Kuo, and J. Y. Chi, *Jpn. J. Appl. Phys.* **45** (2006) L871
[16] D. S. Song, S. H. Kim, H. G. Park, C. K. Kim, and Y. H. Lee, *Appl. Phys. Lett.* **80** (21) (2002) 3901
[17] N. Yokouchi, A. J. Danner, and K. D. Choquette, *IEEE J. Sel. Topics Quantum Electron.* **9** (5) (2003) 1439
[18] J. H. Baek, D. S. Song, I. K. Hwang, K. H. Lee, Y. H. Lee, Y. Ju, T. Kondo, T. Miyamoto, and F. Koyama, *Opt. Express* **12**(5) (2004) 859
[19] A. J. Danner, J. J. Raftery, Jr., P. O. Leisher, and K. D. Choquette, *Appl. Phys. Lett.* **88** (9) (2006) 091114
[20] P. O. Leisher, A. J. Danner, and K. D. Choquette, *IEEE Photon. Technol. Lett.* **18** (20) (2006) 2156
[21] A. M. Kasten, M. P. Tan, J. D. Sulkin, P. O. Leisher, and K. D. Choquette, *IEEE Photon. Technol. Lett.* **20** (23) (2008) 2010

[22] A. M. Kasten, J. D. Sulkin, P. O. Leisher, D. K. McElfresh, D. Vacar, and K. D. Choquett, *IEEE J. Sel. Topics Quantum Electron.* **14** (4) (2008) 1123
[23] T. Czyszanowski, R. P. Sarzala, M. Dems, H. Thienpont, W. Nakwaski, and K. Panajotov, *Phys. Stat. Sol. A* **206** (2009) 1396
[24] T. Czyszanowski, R. P. Sarzala, M. Dems, W. Nakwaski, H. Thienpont, and K. Panajotov, *J. Appl. Phys.* **105** (2009) 093102
[25] D. F. Siriani, P. O. Leisher, and K. D. Choquette, *IEEE J. of Quantum Electron.* **45** (7) (2009) 762
[26] Paul O. Leisher, J. D. Sulkin, and K. D. Choquette, *IEEE J. Sel. Topics Quantum Electron.* **13** (5) (2007) 1290
[27] K. H. Lee, J.-H. Baek, I.-K. Hwang, Y.-H. Lee, G.-H. Lee, J.-H. Ser, H.-D. Kim, and H.-E. Shin, *Opt. Express* **12** (17) (2007) 1301
[28] T. Birks, J. Knight, and P. Russell, *Opt. Lett.* **22** (13) (1997) 961
[29] A. Ferrando, E. Silvestre, J. J. Miret, P. Andres, and M. V. Andres, *Opt. Lett.* **24** (5) (1999) 276.
[30] Z. Zhu, and T. G. Brown, *Opt. Express* **10** (17) (2002) 853
[31] H.-P. D. Yang, I.-C. Hsu, Y.-H. Chang, F.-I. Lai, H.-C. Yu, G. Lin, R.-S. Hsiao, N. A. Maleev, S. A. Blokhin, H.-C. Kuo, and J. Y. Chi, *IEEE J. Sel. Topics Quantum Electron.* **26** (11) (2008) 1387
[32] G. P. Agrawal, *Fiber-Optic Communication Systems* (Wiley, New York, USA 1997)
[33] N. Yokouchi, A. J. Danner, and K. D. Choquette, *Appl. Phys. Lett.* **82** (21) (2003) 1344